

# Theoretical model of errors in micromirror-based three-dimensional particle tracking

Andrew J. Berglund, Matthew D. McMahon, Jabez J. McClelland, and J. Alexander Liddle

*Center for Nanoscale Science and Technology*

*National Institute of Standards and Technology, Gaithersburg, MD 20899, USA*

## Abstract

Several recently-developed particle-tracking and imaging methods achieve three-dimensional sensitivity through the introduction of angled micromirrors into the observation volume of an optical microscope. Here, we model the imaging response of such devices, and show how the direct and reflected images of a fluorescent particle are affected. In particle-tracking applications, asymmetric image degradation manifests itself as systematic tracking errors. Based on our results, we identify strategies for reducing systematic errors to the 10 nm level in practical applications.

PACS numbers:

Optical microscopy and single-particle tracking provide experimental access to nanoscale dynamics in diverse areas, including colloid physics [1], intracellular transport [2], and molecular biophysics [3]. The most widely used version of the technique consists of two-dimensional tracking based on offline analysis of digital images [4]. However, the extension of these methods to localizing and tracking particles in three dimensions is not straightforward, and a significant body of research has been devoted to this problem using various techniques such as astigmatic imaging [5], off-focus imaging [6], holographic microscopy [7], and point-spread function engineering [8]. Recently, a new approach to three-dimensional particle tracking has been developed by several groups [9–13], in which angled mirrors [14] are placed in the object space of a microscope, providing the usual direct image and a complementary reflected image in a plane (nearly) perpendicular to the focal plane. This approach gives 3D information by providing, for example, simultaneous *xy* and *xz* views of the region of interest.

With this new approach, we recently demonstrated three-dimensional tracking of 190 nm fluorescent particles with better than 20 nm repeatability at camera frame rates in excess of 300 Hz, using pyramidal micromirror wells (PMWs) [11]. In that study, we also exploited the redundant information provided by multiple reflected images to evaluate the overall accuracy of the measurement. We found that position-dependent systematic tracking errors contributed an uncertainty of approximately 20 % of a trajectory’s extent, suggesting absolute errors of several hundred nanometers over few-micron trajectories. While micromirror-based methods are promising for 3D, nanometer-scale metrology, errors of this magnitude threaten their utility.

In this Letter, we investigate the origin of these systematic errors in micromirror-based three-dimensional particle tracking. We calculate the image of a particle reflected from an angled micromirror, accounting for optical aberrations and the fact that the mirror creates an asymmetric entrance pupil that removes the space-invariance of the system’s optical response. We find that systematic errors are predominantly due to angular truncation within the imaging system, where the degree of truncation depending on the particle’s position, the micromirror geometry, and the details of the optical system. These factors contribute to position-dependent image distortions and a corresponding deviation between a particle’s true position and the apparent position of its reflection, likely an example of the fundamental tradeoff between axial resolution and lateral shift invariance [15]. Our

calculations suggest a mitigating strategy: by using lower numerical aperture (NA) imaging conditions, fabricating PMWs with wider opening angles, or imaging particles that are deep within a PMW, deleterious effects are suppressed and systematic tracking errors can be reduced to the 10 nm level.

In order to analyze tracking errors, we must calculate the reflected image of a particle near an angled reflective surface. Two components contribute to the overall reflected image: the geometric occlusion of certain rays by the angled micromirror, and the native diffractive aberrations of the imaging system. For the geometric component, we evaluate the effect of the mirror geometry on the imaging system. For the diffractive component, we use the scalar method of Gibson and Lanni [16] to model the aberrations resulting from the microscope optics, sample medium, and cover glass. Closely related geometric effects have been studied in Ref. [17], though reflected images and aberrations were not considered.

The geometry of our calculation is shown in Fig. 1. The particle position is  $\mathbf{p}$  and the mirror surface has unit normal vector  $\hat{\mathbf{n}}$  and passes through some point  $\mathbf{v}$ . In a well-corrected imaging system, each Cartesian point  $(\xi, \eta)$  in the back focal plane (BFP) corresponds to a propagation direction  $\hat{\mathbf{u}}$  within the sample. It is convenient to use normalized cylindrical coordinates  $(\rho, \phi)$  in the BFP, with  $\xi = \rho R \cos \phi$  and  $\eta = \rho R \sin \phi$ .  $R$  is the radius of an extremal ray, which for a system with back focal length  $f$  and magnification  $M$  satisfies  $R = \text{NA}f/M$ , so that the field amplitude is nonzero only in the BFP region  $\rho \leq 1$ . The correspondence between  $(\rho, \phi)$  and  $\hat{\mathbf{u}}$  can be deduced from the Abbe sine condition [16]:  $\hat{\mathbf{u}}(\rho, \phi) = (\sin \theta_s \cos \phi, \sin \theta_s \sin \phi, \cos \theta_s)$  with  $\sin \theta_s = \rho \text{NA}/n_s$  and  $n_s$  the refractive index of the specimen. The geometry of the mirror then determines whether any reflected ray propagates from the particle position  $\mathbf{p}$  into the optical system along  $\hat{\mathbf{u}}$  and hence reaches  $(\rho, \phi)$  in the BFP. For a mirror of infinite extent, direct and reflected rays reach  $(\rho, \phi)$  in the BFP whenever  $\hat{\mathbf{u}}(\rho, \phi) \cdot \hat{\mathbf{n}} > 0$ . For a mirror with finite extent, however, we must formulate additional criteria to determine whether a particular ray reaches the BFP. Let  $\epsilon_{\mathbf{p}} = (\mathbf{p} - \mathbf{v}) \cdot \hat{\mathbf{n}}$  be the (assumed positive) distance of the particle from the mirror surface. The reflected virtual image of the particle appears to originate from the position  $\mathbf{p}_r$  given by the law of reflection,  $\mathbf{p}_r = \mathbf{p} - 2\epsilon_{\mathbf{p}}\hat{\mathbf{n}}$ . One then finds that a ray leaving  $\mathbf{p}$  and reflecting off an infinite mirror at the point  $\mathbf{t}_r = \mathbf{p}_r + \epsilon_{\mathbf{p}}\hat{\mathbf{u}}/(\hat{\mathbf{u}} \cdot \hat{\mathbf{n}})$  propagates along the direction  $\hat{\mathbf{u}}(\rho, \phi)$  and consequently reaches  $(\rho, \phi)$  in the BFP. Therefore, we must only determine whether the reflection point  $\mathbf{t}_r$ , which is itself a function of  $(\rho, \phi)$  through  $\hat{\mathbf{u}}$ , lies within the extent of the

finite mirror. Specializing to a simple geometry where the mirror surface extends from  $z_1$  to  $z_2$ , we find that a reflected ray reaches  $(\rho, \phi)$  in the BFP whenever  $\rho \leq 1$ ,  $\hat{\mathbf{u}} \cdot \hat{\mathbf{n}} > 0$ , and  $z_1 < \mathbf{t}_r \cdot \hat{\mathbf{z}} < z_2$ .

We model diffractive effects, following Ref. [16], by calculating the optical path difference between an aberrated and unaberrated ray originating from  $\mathbf{p}_r$  and reaching  $(\rho, \phi)$  in the BFP. This optical path difference  $W_{\mathbf{p}_r}(\rho)$  is independent of the mirror geometry, and is a function only of  $\rho$  and the reflected position  $\mathbf{p}_r$ , along with the parameters of the optical system such as the refractive indices and thicknesses of the sample, cover glass, and immersion medium. Combining diffractive and geometric effects, we now find the reflected image  $I_r(x, y)$  by Fourier transforming the amplitude in the BFP [18]:

$$I_r(x, y) = \left| \iint_{\mathcal{S}_r} d\xi d\eta A_r e^{ikW_{\mathbf{p}_r}(\rho) - i\frac{k}{f}[(x - M\mathbf{p}_r \cdot \hat{\mathbf{x}})\xi + (y - M\mathbf{p}_r \cdot \hat{\mathbf{y}})\eta]} \right|^2$$

where  $\mathcal{S}_r$  is the set of points satisfying  $\rho \leq 1$ ,  $\hat{\mathbf{u}} \cdot \hat{\mathbf{n}} > 0$ , and  $z_1 < \mathbf{t}_r \cdot \hat{\mathbf{z}} < z_2$ .  $A_r$  is an amplitude factor, which we take to be constant. An angle-dependent reflectivity or apodization factor could be included in  $A_r$ , but we leave these considerations to a more refined vector calculation that also includes polarization effects [19, 20]. The direct image can also be distorted by the presence of the mirror, though we have found this to be a negligible effect. Similar reasoning to that described above shows that the direct is found from the same equation, by replacing  $W_{\mathbf{p}_r}(\rho)$  with  $W_{\mathbf{p}}(\rho)$  and integrating over the region  $\mathcal{S}_d$ , the set of points satisfying  $\rho \leq 1$ , but *not* ( $\hat{\mathbf{u}} \cdot \hat{\mathbf{n}} < 0$  and  $z_1 < \mathbf{t} \cdot \hat{\mathbf{z}} < z_2$ ), where  $\mathbf{t} = \mathbf{p} - \epsilon_{\mathbf{p}} \hat{\mathbf{u}} / (\hat{\mathbf{u}} \cdot \hat{\mathbf{n}})$ .

In Fig. 2, we show measured and calculated images showing *four* reflections of a particle in a pyramidal micromirror well. The figure shows good qualitative correspondence between the observed (a) and calculated (c) distorted images. To quantitatively evaluate the 3D tracking error resulting from image distortion, we calculated the center-of-mass deviation between distorted and undistorted images of a particle near a single micromirror, with normal vector in the  $xz$  plane. Results are shown in Fig. 3, which reveals the shape of the “usable” particle tracking region for various mirror depths, numerical apertures, and mirror angles  $\theta$ . Although the exact values of the systematic error will generally depend on all parameters of the system, we can nevertheless draw a number of general conclusions. First, the tracking error is smaller for particles deeper inside a PMW, *i.e.* farther from the top

edge. Second, decreasing the mirror angle  $\theta$  or increasing the numerical aperture gives more severe tracking errors. Several scenarios with significant regions of 3D tracking error below 10 nm are predicted in Fig. 3.

In summary, we have calculated images and systematic tracking errors for a particle near an angled, reflective surface in an optical microscope. For three-dimensional particle tracking applications, we predict that systematic errors can be reduced by imaging deep within a micromirror well, reducing the numerical aperture, and increasing the mirror angle. The method presented here should facilitate calculation of the direct-plus-reflected point spread function necessary as a deconvolution kernel for three-dimensional imaging applications [21].

---

- [1] S. K. Sainis, V. Germain, and E. R. Dufresne, Phys. Rev. Lett. **99**, 018303 (2007).
- [2] M. Dahan, S. Levi, C. Luccardini, P. Rostaing, B. Riveau, and A. Triller, Science **302**, 442–445 (2003).
- [3] A. Yildiz, J. N. Forkey, S. A. McKinney, T. Ha, Y. E. Goodman, and P. R. Selvin, Science **300**, 2061–2065 (2003).
- [4] J. Crocker and D. Grier, J. Colloid Interface Sci. **179**, 298–310 (1996).
- [5] H. Kao and A. Verkman, Biophys. J. **67**, 1291–1300 (1994).
- [6] M. Speidel, A. Jonáš, and E.-L. Florin, Opt. Lett. **28**, 69–71 (2003).
- [7] F. C. Cheong, B. Sun, R. Dreyfus, J. Amato-Grill, K. Xiao, L. Dixon, and D. G. Grier, Opt. Express **17**, 13071–13079 (2009).
- [8] S. Pavani and R. Piestun, Opt. Express **16**, 22048–22057 (2008).
- [9] K. T. Seale, R. S. Reiserer, D. A. Markov, I. A. Ges, C. Wright, C. Janetopoulos, and J. P. Wikswo, J. Microsc. **232**, 1–6 (2008).
- [10] S. Choi and J.-K. Park, Appl. Phys. Lett. **93**, 191909 (2008).
- [11] M. D. McMahon, A. J. Berglund, P. Carmichael, J. J. McClelland, and J. A. Liddle, ACS Nano **3**, 609–614 (2009).
- [12] K. Seale, C. Janetopoulos, and J. Wikswo, ACS nano **3**, 493–497 (2009).
- [13] H. Hajjoul, S. Kocanova, I. Lassadi, K. Bystricky, and A. Bancaud, Lab on a Chip **9**, 3054–3058 (2009).
- [14] M. Trupke, F. Ramirez-Martinez, E. Curtis, J. Ashmore, S. Eriksson, E. Hinds, Z. Moktadir,

- C. Gollasch, M. Kraft, G. Prakash, J. Baumberg, Applied Physics Letters **88**, 071116 (2006).
- [15] S. B. Oh and G. Barbastathis, Appl. Opt. **48**, 5881–5888 (2009).
  - [16] S. Gibson and F. Lanni, J. Opt. Soc. Am. A **8**, 1601–1613 (1991).
  - [17] S. Lindek, J. Swoger, and E. Stelzer, J. Mod. Opt. **46**, 843–858 (1999).
  - [18] J. Goodman, *Introduction To Fourier Optics* (McGraw-Hill, New York, 1996).
  - [19] B. Richards and E. Wolf, Proc. Roy. Soc. London **253**, 358–379 (1959).
  - [20] P. Török, P. Varga, Z. Laczik, and G. Booker, J. Opt. Soc. Am. A **12**, 1605–1605 (1995).
  - [21] J. G. McNally, T. Karpova, J. Cooper, and J. A. Cochello, Methods **19**, 373–385 (1999).

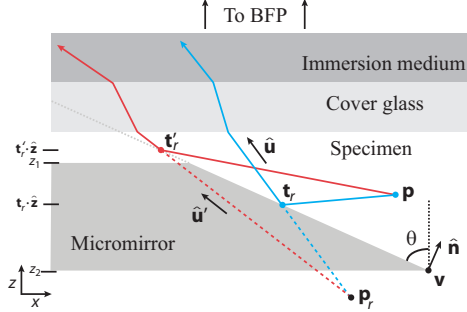


FIG. 1: Geometry of the model. The ray along direction  $\hat{\mathbf{u}}$  reflects off the micromirror at  $\mathbf{t}_r$  and eventually reaches the BFP. No ray leaving along  $\hat{\mathbf{u}}'$  reaches the BFP because the reflection point  $\mathbf{t}'_r$  lies outside the finite extent of the mirror ( $\mathbf{t}'_r \cdot \hat{\mathbf{z}} > z_1$ ).

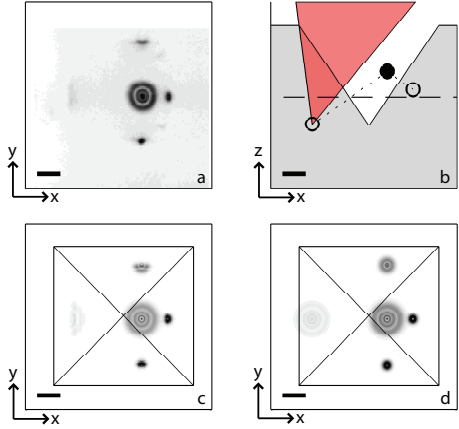


FIG. 2: Observed and calculated images of a particle in a PMW. (a) Measured image of a 190 nm diameter fluorescent microparticle in a PMW ( $\theta = 35^\circ$ , imaged with NA 0.95/40X air objective), showing the direct and four reflected images. (b)  $xz$  cross-section section of the geometry used for calculations (c-d). The collected light cone is asymmetrically truncated by the mirror on the left and by the NA on the right. The particle and mirror positions are estimated from analysis of (a), while unknown experimental parameters such as the position of the focal plane (dashed line) are chosen by hand. (c) Calculated images as described in the text, modified to account for truncation by the four triangular PMW faces. (d) “Perfect” images, which would arise if microscope aberrations were present but there was no truncation of rays by the mirror. Other parameters: specimen index  $n_s = 1.47$  (a 4:1 glycerine-water mixture), coverglass ( $n_g = 1.5$ ),  $2\pi/k = 550$  nm. To represent a spherical aberration correction collar on the objective, the calculations use an index-matched immersion medium  $n_i = 1.5$ . The contrast is enhanced equally in (a), (c), and (d) to aid in viewing the weaker reflections. Scale bar: 5  $\mu\text{m}$ .

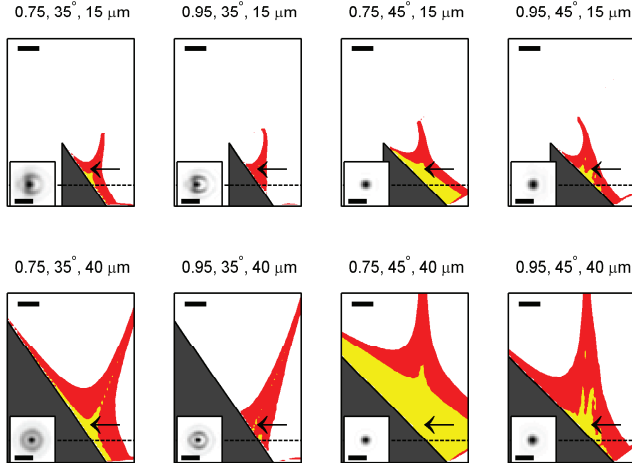


FIG. 3: Contour plots showing the regions where absolute tracking errors are below 10 nm (lighter region, yellow online) and below 250 nm (darker region, red online) for various scenarios. For each plot, the NA, mirror angle  $\theta$ , and mirror depth  $z_1 - z_2$  are shown at the top. The reflected image of a particle is calculated at each position, and the center of mass of the brightest 95% of the reflection is determined; the 3D position is reconstructed using this value as the reflected position, and the resulting tracking error is recorded. Scale bar: 5  $\mu\text{m}$ . The insets show the calculated reflection at the point indicated by the arrow (scale bar 1  $\mu\text{m}$ ). Other parameters:  $n_s = 1.33$ ,  $n_g = 1.5$ ,  $n_i = 1.5$ ,  $2\pi/k = 550 \text{ nm}$ .